Journal of Luminescence 192 (2017) 860–866

Contents lists available at ScienceDirect

Journal of Luminescence

journal homepage: www.elsevier.com/locate/jlumin

The shell thickness and surface passivation dependence of fluorescence decay kinetics in CdSe/ZnS core-shell and CdSe core colloidal quantum dots

Ruwini D. Rajapaksha, Mahinda I. Ranasinghe*

Department of Chemistry, New Mexico Institute of Mining and Technology, Socorro, NM 87801, USA

ARTICLE INFO

Keywords:
Core-shell quantum dots
CdSe
CdSe/ZnS
Time-resolved fluorescence upconversion spectroscopy
Fluorescence lifetime

ABSTRACT

Femtoseconds, ultrafast, time-resolved, fluorescence upconversion spectroscopy was utilized to investigate the photo-induced emission decay dynamics of CdSe and CdSe/ZnS colloidal quantum dots whose surfaces were stabilized with octadecyl amine (ODA). The studies focused on understanding the influence of the surface stabilizing group on the fluorescence decay dynamics of CdSe and CdSe/ZnS and the effect of shell thickness on the photo-physical properties of core-shell quantum dots. The Core-shell materials showed excellent photostability, longer rise times, and lengthy decay times.

1. Introduction

Semiconductor nanocrystals have been studied for many years due to their optical and electronic properties; these properties can be manipulated by their size, shapes, and capping ligands. Due to the quantum confinement effect, semiconductor colloidal quantum dots (CQDs) have attracted significant interest among the scientific community because of their unique optical and electronic properties [1]. The core-shell CQDs were introduced to enhance the photostability of single quantum dots by coating them with a protective layer that has a higher band gap than the CQD [2]. These protective layers can be either an inorganic or organic materials [3]. The inorganic materials such as ZnS are more durable than organic materials and are known to help improve the photoluminescence quantum yield by passivating non-radiative surface trap sites [3]. Therefore, these colloidal semiconductor materials are attractive candidates for various applications such as solar cells [4–7], photovoltaics [8,9], light emitting diodes [10–13], and biolabeling for medicinal applications [14–16]. A better understanding of the excited state photophysical kinetics, dynamics, electronic properties, and optical properties of these core-shell CQDs is crucial for their use in these applications.

Many studies have used CdSe and CdSe/ZnS core-shell CQDs [17–26], but there are only a few studies that have reported on fluorescence decay dynamics, utilizing time-resolved fluorescence upconversion spectroscopy [8,11,27–29]. The fluorescence upconversion spectroscopic study is the ideal technique to investigate these CQDs systems because it can probe excited state fluorescence dynamics without interfering with other processes, such as excited state absorption and ground state recovery [30]. We believe it is important and crucial to investigate the size dependent variation of fluorescence decay dynamics of the CdSe core-only CQDs and CdSe/ZnS core-shell CQDs and also the effect of shell thickness on fluorescence decay dynamics in core-shell CQDs using ultrafast, time-resolved, fluorescence upconversion spectroscopy inorder to use them in potential applications. We believe this kind of study will give a better understanding of the passivation of trap sites, enhance fluorescence lifetime, and Photo luminescent (PL) quantum yield of a single CQD by enhancing the photostability via the inorganic shell.

In this article, the findings of a systematic investigation of size dependent fluorescence decay properties of several core-only and core-shell CQDs using ultrafast, time-resolved, fluorescence upconversion spectroscopy are reported. Here, our main goal is to investigate the size and the shell thickness dependence of fluorescence decay dynamics on CdSe and CdSe/ZnS core-shell CQDs using ultrafast time resolved fluorescence spectroscopy. When selecting the CQD systems, we intended to include a new dimension to our investigation, while maintaining the focus on our main goal. We selected to study new CdSe/ZnS CQD systems with a different surface stabilizing group, which is not reported or studied in depth in the literature. Capping ligands in CQD systems play a crucial role in preventing coagulation of CQDs, surface oxidation, and changing their optical and electronic properties. According to our knowledge, the widely used capping ligands are trioctylphosphine (TOP), trioctylphosphine oxide (TOPO) and hexadecyl amine (HAD) [2,8,17,22,27,28,31]. For our studies we selected completely different CQD systems that are capped with octadecyl amine (ODA). With this novel capping ligand ODA, which has the longest alkyl

* Corresponding author.
E-mail address: mahinda.ranasinghe@nmt.edu (M.I. Ranasinghe).

http://dx.doi.org/10.1016/j.jlumin.2017.08.024
Received 24 October 2016; Received in revised form 6 February 2017; Accepted 11 August 2017
Available online 12 August 2017

Table 1
The size distribution of CdSe (CSE) and CdSe/ZnS (CZ) QDs.

Sample	Size/nm	
CSE500	2.3–2.4	
CSE540	2.6–3.0	
CSE580	3.5–4.0	
CSE600	4.3–4.7	
CSE620	5.2–6.2	
CSE640	6.2–7.7	
CZ500	Core: 2.0–2.5	Shell: 2.0
CZ540	Core: 2.8	Shell: 3.3
CZ580	Core: 3.6	Shell: 4.0
CZ600	Core: 4.0	Shell: 4.3
CZ620	Core: 4.5	Shell: 4.5
CZ640	Core: 4.8	Shell: 4.7

chain (C_{18}) among the usual capping ligands that is not reported in the literature. We intend to provide the impact of ODA capping ligand on the optoelectronic properties and photophysical dynamics of CdSe and CdSe/ZnS CQD systems.

Our research team believes, this fluorescence decay dynamics studies will provide knowledge to fill the gap between past and present research works by providing detailed insight of CdSe and CdSe/ZnS CQDs photophysical properties and probing the higher excitation dynamics. It should be mentioned that the theoretical investigation has shown strong excitonic intersections in the core-shell CQDs [32]. Similarly, we believe our investigations will complement the work that has been done by other renowned researches in the field [17,20,23,33–40].

2. Materials and methods

For the study given in this article, two sets of six samples of ODA capped CdSe and CdSe/ZnS CQDs having the same absorptions and emissions were purchased from NN Labs. The sizes of the QDs used in this study are shown in Table 1.

The CQD samples were dispersed in toluene. The absorption measurements were performed using CARY 60 UV–VIS spectrophotometer and steady state fluorescence measurements were obtained by using the SHIMADZU RF-5301PC spectrofluorometer. The time-resolved fluorescence upconversion studies were performed utilizing the NEWPORT time-resolved fluorescence spectrometer (TRFLS) that is shown in Fig. 1. The TRFLS is a hybrid fluorescence upconversion and time-correlated single photon counting instrument. In this iteration of TRFLS, the fundamental output beam from the oscillator (Spectra Physics Mai Tai HP) is split in to two. One portion is sent to generate a second or third harmonic excitation beam (Spectra Physics / GWU UHG) and the residual served as the gate for upconversion. The gate beam is passed to a gold coated broadband hollow retroreflector with < 1″ parallelism (Newport UBBR2.5-1I) mounted on a computer controlled translation stage (New-port ILS250CC). The beam makes four passes up and down the stage, resulting in a maximum delay time of 3.3 ns. The gate beam is focused by an antireflection coated lens (New-port AR.16) onto the upconversion crystal (BBO, type I). The fluorescence pump beam enters the TRFLS enclosure separately and has polarization set by a broadband UV–VIS wave plate, and is focused onto the sample by an UV–VIS antireflection coated lens. The fluorescence is collected and collimated by a visible achromatic aspheric lens. The residual pump light is removed by a dielectric long pass filter. The fluorescence is turned and focused onto the upconversion crystal by an achromatic lens. The fluorescence and gate cross at a small angle (< 10°) in the upconversion crystal. The upconversion crystal is mounted on a motorized rotation stage and the phase matching angle is controlled automatically by the software after the generation of a tuning curve depending on the wavelength of the gate beam and fluorescence. The upconverted fluorescence is filtered to remove

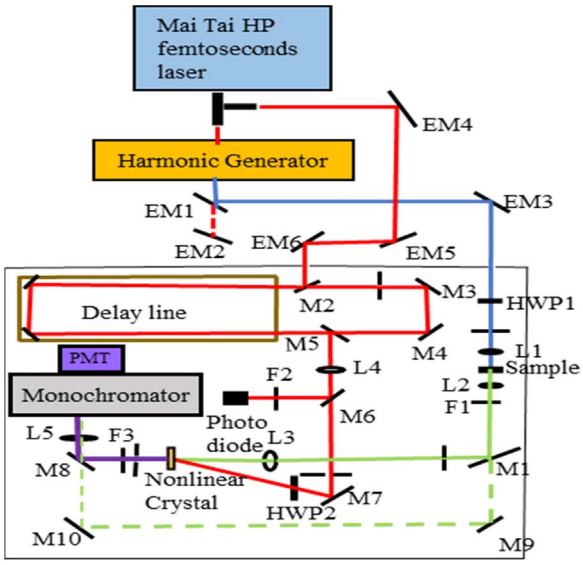

Fig. 1. TRFLS layout, red lines indicate the gate beam (800 nm), blue lines represent the excitation beam, green lines are the fluorescence beam and purple lines are upconverted beam. EM1-6 are external mirrors, HWP1-2 are half wave plates, M1-10 are mirrors, L1-5 are lenses, and F1-3 are filters. (For interpretation of the references to color in this figure legend, the reader is referred to the web version of this article.)

contributions from the second harmonic of the gate and of the fluorescence using a combination of colored glass and dielectric filters and is focused into a computer controlled monochromator (Newport CS130) by an ultraviolet-let antireflection coated lens (Newport AR.10). The monochromator input and output slits are variable and are controlled by micrometer. The upconverted light is resolved as a wavelength and is detected by a PMT optimized for photon counting in the ultraviolet region of the spectrum (Hamamatsu). The single photons are counted by a time-correlated single photon counting (TCSPC) board (Becker & Hackle) and displayed in the TRFLS software or recorded in a file when acquiring data.

3. Experimental

The time-resolved, fluorescence upconversion experiments were carried out as follows: 1.0 mL of 1 mg/mL of CQD sample was placed into a rotating cell (50 rpm). The cell constructed by placing a 1 mm thickness teflon spacer between two quartz plates, and we placed the sample in between two quartz plates. Two teflon spacers were placed on top and bottom of these quartz plates and this was inserted and tighten to a rotating compartment. The gate beam was set to 800 nm and a 400 nm excitation beam was generated using SHG. All samples were excited at an excitation power of 35 mW. The fluorescence beam and the gate beam were directed to overlap within the nonlinear crystal. The nonlinear crystal was rotated to get the maximum phase matching angle and hence the maximum upconversion signal. The upconverted signal was generated by mixing the fluorescence and fundamental frequencies in BBO crystal. This is done by generating the sum frequencies of the gate and the fluorescence beams as represented in Eq. (1),

$$\lambda_{upconverted}{}^{-1} = \lambda_{gate}{}^{-1} + \lambda_{fluorescence}{}^{-1} \quad (1)$$

Instrumental response function (IRF) was determined by placing water into the rotating cell and upconverting the scattered excitation beam with the gate beam. IRF was calculated to be ~ 80 fs fwhm. For all samples, upconversion spectra were generated for parallel polarizations of excitation by doing at least five scans for the first 40 ps. All the scans for a given wavelengths were added, averaged, and normalized. The decay fit was done using second order decay equation, shown in Eq. (2). The A_1, A_2 are amplitudes associated with decays and τ_1, τ_2

are the decay constants.

$$y = A_1\, exp\left(\frac{-x}{\tau_1}\right) + A_2\, exp\left(\frac{-x}{\tau_2}\right) + y_0 \quad (2)$$

The fluorescence lifetime (τ_{FL}) of the CQD samples were measured using Horiba Fluorolog TCSPC instrumentation. All samples were excited using 360 nm nano LED diode and collected emitted fluorescence at each respective emission wavelengths of studied CQDs. Lifetimes were calculated fitting into two exponential decay function, which is mentioned above in the Eq. (2).

Photoluminescence (PL) quantum yields were calculated using 1 mg/mL coumarin 153 (C153) in an ethanol solution. This was taken as a known reference for PL quantum yield calculations, measuring the emissions by exciting at the same excitation wavelength used to excite CQDs. The emission wavelength range was set as the same emission range used for the above CQDs samples which was 410 − 780 nm. The fluorescence quantum yield was calculated using the equation showing in the Eq. (3). In the Eq. (3), QY is the PL quantum yield of the CQD samples and QY_{ref} is the PL quantum yield of the reference sample which is 0.5444 for C153. η^2 is the refractive index of the solvent used for the CQDs. Here, the CQDs were dispersed in toluene and the refractive index for toluene is 1.4968. η^2_{ref} is the refractive index of the solvent of the reference sample and for our case the solvent is ethanol and the refractive index of ethanol is 1.3616. I and I_{ref} are the integrated fluorescence intensities of the CQDs and the reference sample respectively. Finally, A and A_{ref} are the absorbance of the CQDs and the reference sample at the excitation wavelength.

$$QY = QY_{ref}\frac{\eta^2}{\eta^2_{ref}}\frac{I}{A}\frac{A_{ref}}{I_{ref}} \quad (3)$$

From measured fluorescence lifetime (τ_{FL}) and calculated PL quantum yields (QY), the radiative lifetime (τ_r) and nonradiative lifetime (τ_{nr}) were calculated using the Eqs. (4) and (5) mentioned in below.

$$\tau_r = \frac{\tau_{FL}}{QY} \quad (4)$$

$$\frac{1}{\tau_{nr}} = \left(\frac{1}{\tau_{FL}} - \frac{1}{\tau_r}\right) \quad (5)$$

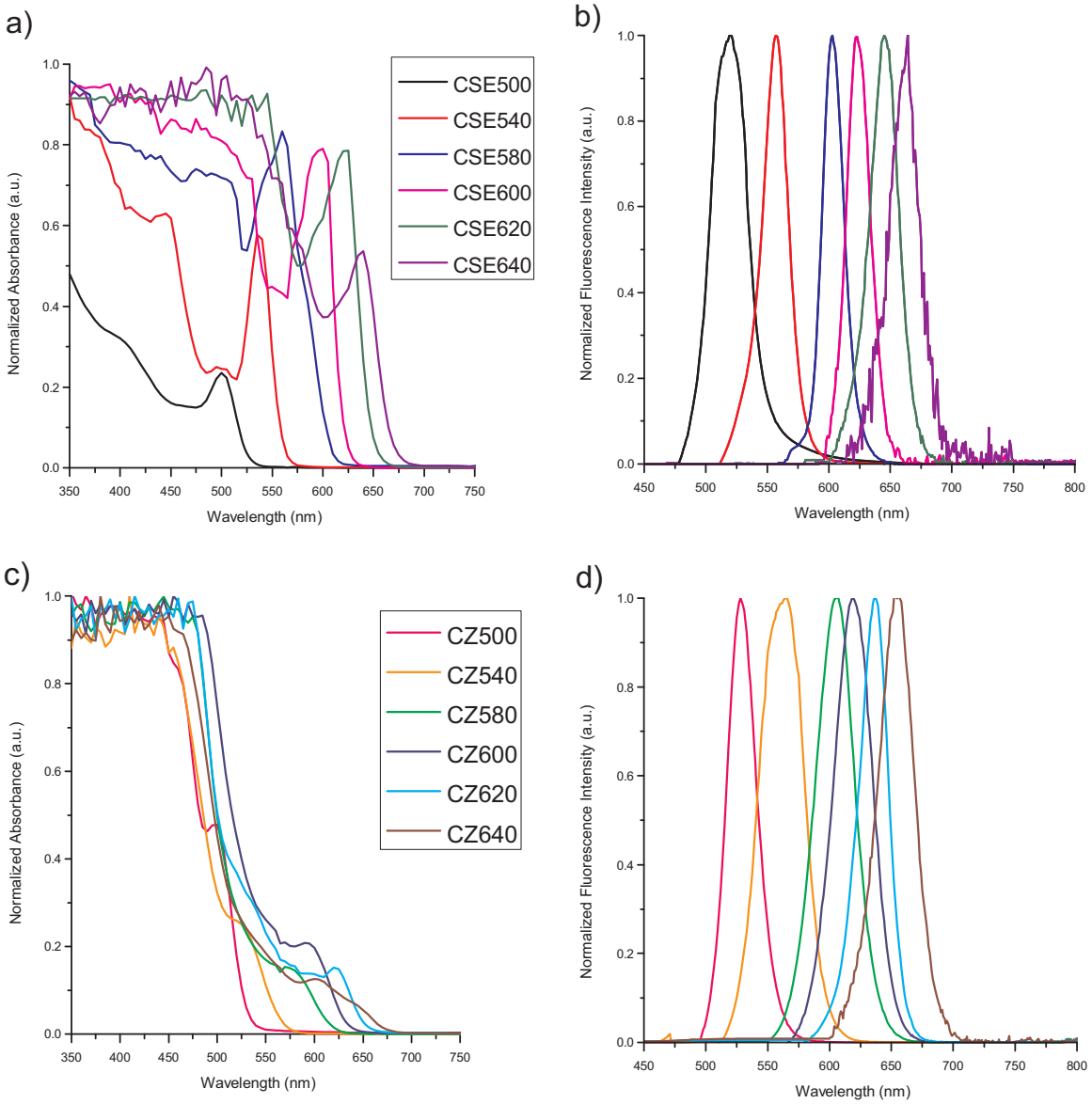

Fig. 2. Normalized UV–Vis absorbance spectra of a) CdSe, c) CdSe/ ZnS and fluorescence (λ_{ex} at 400 nm) spectra of b) CdSe, d) CdSe/ZnS CQDs in toluene.

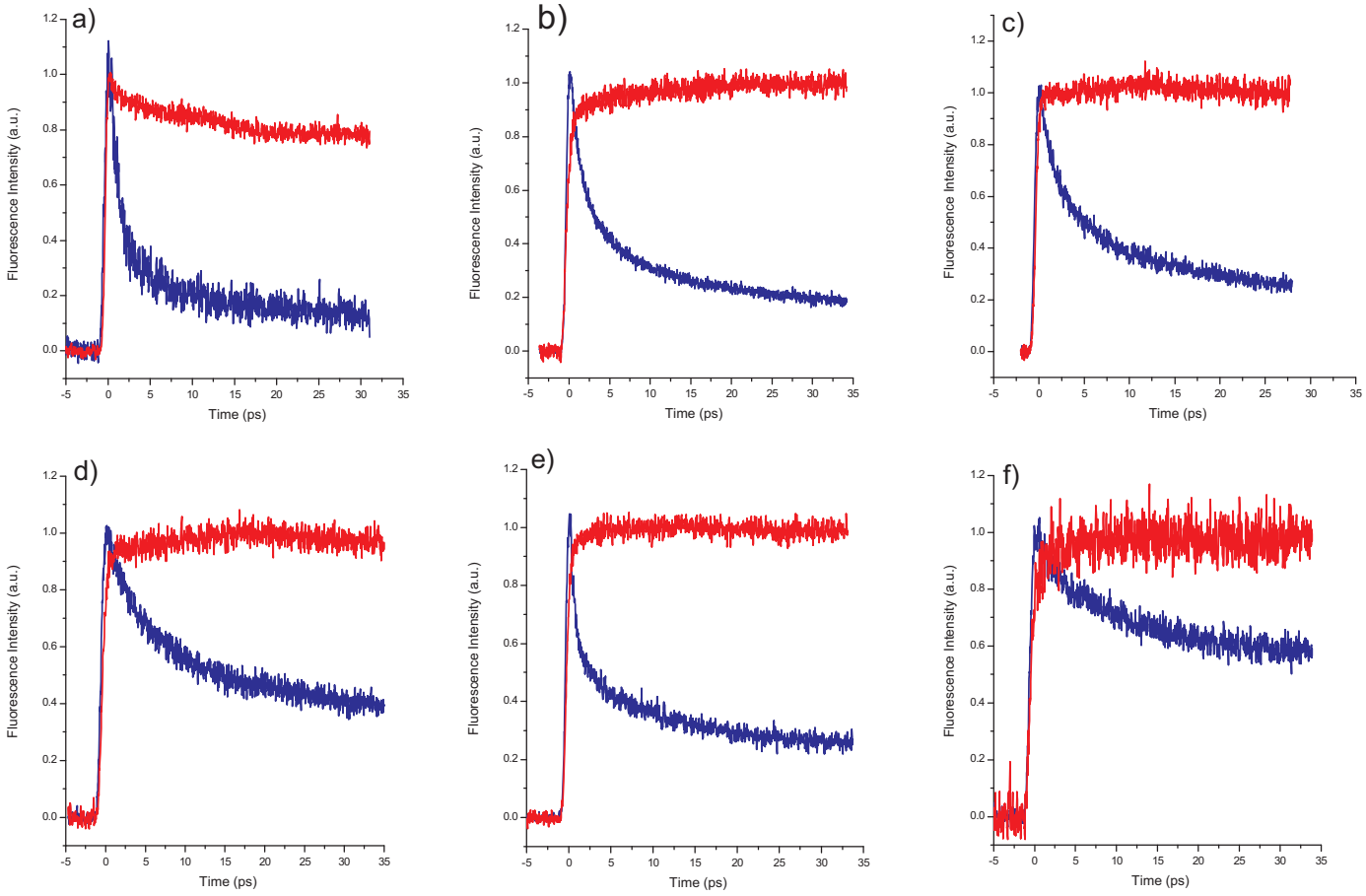

Fig. 3. Normalized time-resolved, fluorescence decay spectra of a) CSE500 and CZ500 (λ_{em} 520 nm), b) CSE540 and CZ540 (λ_{em} 540 nm), c) CSE580 and CZ580 (λ_{em} 604 nm), d) CSE600 and CZ600 (λ_{em} 632 nm), e) CSE620 and CZ620 (λ_{em} 640 nm), f) CSE640 and CZ640 (λ_{em} 670 nm). The blue line graphs represent decay profile of CdSe materials and red graphs represent decay profile of CdSe/ZnS core/shell materials excitation with 3.102 eV. (For interpretation of the references to color in this figure legend, the reader is referred to the web version of this article.)

4. Results and discussion

Fig. 2 shows the absorption and emission spectra of the samples investigated. The absorption measurements of six CdSe CQD samples showed absorption maxima at 500, 540, 580, 600, 620, and 640 nm. The excitation of these samples at 400 nm showed the fluorescence maxima at 520, 557, 605, 623, 645, and 663 nm respectively. Similarly, CdSe/ZnS showed absorption maxima at 500, 540, 580, 600, 620, and 640 nm and respective fluorescence emission maxima at 520, 565, 607, 620, 637, and 655 nm with 400 nm excitation.

The excitation with 3.102 eV results in populating the higher energy states of most of the studied CQDs except CSE500 (4.22 eV) and CSE540 (3.45 eV). As shown in Fig. 3, the upconverted fluorescence emission decay dynamics of CdSe and CdSe/ZnS showed two different distinct decay profiles.

The CdSe CQDs showed multi exponential decay while the CdSe/ZnS CQDs showed very different decay kinetics. In the case of CdSe core-only CQDs, the fluorescence decay, showed a fast decay component and a slower decay component. Whereas, the fluorescence decay of CdSe-ZnS core-shell CQDs did not show a fast fluorescence decay component.

CdSe/ZnS CQDs show the longer rise times and a longer fluorescence decay component. This is because of the ZnS shell passivates the nonradiative trap states on CdSe core making the core more photo stable [24,41]. These observations clearly suggest that the shell of core-shell CQDs plays a key role in determining the photophysical properties of these core-shell CQDs. Inorder to obtain the fluorescence decay kinetic data, the fluorescence decay of CdSe and CdSe/ZnS core-shell CQDs was fitted with the two exponential decay function given in Eq. (2), by deconvoluting with the IRF. Fig. 3 also shows the change in the fluorescence decay profiles with core and core-shell materials even though they have the same absorptions and emissions. The CdSe/ZnS also showed fluorescence decay profiles, which have a range of size-dependent rise times. Similarly, the ZnS capped core-shell CQDs show good photostability [24,41] and the longer decay can be attributed to the quenching of non-radiative recombination processes at the surface of the luminescent CdSe core.

The calculated fitting parameters for fluorescence decay using fluorescence upconversion studies are given in Table 2.

According to the data shown in the Table 2, the ODA capped CdSe

Table 2
Calculated fitting parameters from fluorescence upconversion studies.

Sample	A_1	A_2	τ_1 / ps	τ_2 / ps
CSE500	0.78	0.22	1.19	10.46
CSE540	0.57	0.33	1.56	11.58
CSE580	0.44	0.37	1.86	12.71
CSE600	0.36	0.33	3.69	21.65
CSE620	0.57	0.30	0.70	10.35
CSE640	0.12	0.33	1.95	12.33
CZ500	0.17	0.07	11.97	0.64
CZ540	− 0.10	− 0.95	11.34	0.60
CZ580	− 0.04	− 0.88	4.18	0.42
CZ600	− 0.06	− 0.85	5.73	0.60
CZ620	− 0.04	− 0.97	2.24	0.45
CZ640	− 0.11	− 0.89	3.60	0.59

Table 3
The calculated PL quantum yield (QY), fluorescence lifetime (τ_{FL}), radiative lifetime (τ_r) and nonradiative lifetime (τ_{nr}) data.

Sample	QY	τ_{FL} / ns	τ_r / ns	τ_{nr} / ns
CSE500	0.456	0.577	1.27	1.06
CSE540	0.489	1.60	3.27	3.13
CSE580	0.336	9.41	28.0	14.2
CSE600	0.322	14.0	43.4	20.7
CSE620	0.398	10.2	25.6	16.9
CSE640	0.392	41.9	106.9	68.9
CZ500	0.604	10.6	17.5	26.8
CZ540	0.640	17.7	27.7	49.2
CZ580	0.505	41.4	82.0	83.7
CZ600	0.476	41.8	87.8	79.8
CZ620	0.377	37.7	99.9	60.6
CZ640	0.293	25.4	86.6	35.9

CQD has a fast decay component due to the short-lived species with time constant $\tau_1 \sim 1$–3 ps. It should be noted that ODA capped CdSe core-only CQD with the same size follows a similar trend reported in the literature with different capping ligands [28,31]. Both of these decay components showed a gradual lengthening of the decay times with size of the CQD. In our study, we observed shorter decay followed by a longer decay for CdSe/ZnS materials, which may be due to passivating of non-radiative e^-/h^+ recombination at the defect sites on the CdSe surface. To gain a clear understand about photophysical dynamics, it is necessary to calculate radiative and nonradiative lifetimes using calculated PL quantum yields and calculated fluorescence lifetimes. From TCSPC studies we calculated the fluorescence lifetime and combining Eqs. (3)–(5) we calculated the radiative and nonradiative lifetimes of studied CQDs. The calculated PL quantum yields (QY), fluorescence lifetimes (τ_{FL}), radiative lifetimes (τ_r) and nonradiative lifetimes (τ_{nr}) are shown in the Table 3. The fluorescence lifetime (τ_{FL}) of these materials were calculated taking the average of three trials.

According to the Table 3, the core-shell CQDs show increase of PL quantum yields compared to the core-only CQDs. This is because the passivation of nonradiative recombination sites on core by the ZnS shell [2]. Furthermore, the greatest PL quantum yield of core-shell CQDs ~ 64% may be due to the surface capping group ODA. We believe that ODA plays a crucial role in influencing the PL quantum yield of these studied CQDs. Moreover, according to the Table 3, we observed an increase of PL quantum yield of core-shell CQDs up to a certain shell thickness (CZ540), PL quantum yield ~ 64% and started to decrease and further decreased up to ~ 29.3% with an increase of shell thickness. This is a similar trend observed by Dabbousi et al. working with CdSe/ZnS core-shell CQDs with different ZnS monolayer coverages [2]. This decrease of PL quantum yield in thicker shells can be due to defects in the ZnS shell [2,42,43]. We observed that any further increase in the shell thickness after the sample CZ600 causes the decrease of fluorescence lifetime in core-shell materials. As shown in Table 3, in core-shell materials, the fluorescence lifetime increases up to sample CZ600, which has a 4.3 nm shell thickness. After that shell thickness, the fluorescence lifetimes started to decrease. For the sample CZ620 with 4.5 nm shell it decreases and further decreases for the sample CZ640, which has the thicker shell among all core-shell CQD samples studied. The radiative lifetime of all CQD sample increase. This may be due to the increase of photo excited excitons going through the hole trapping pathways making the radiative processes more dominant [11]. Increase of radiative lifetimes in core-shell CQDs can be attributed to the increase of trap emissions with increase of shell thickness due to lattice strain and non-uniformity of shells [2,38,44]. Similarly, we can see the increase of nonradiative lifetime for core-shell materials up to the sample CZ580, followed by decrease slightly and further decreased with increase of shell thickness. The increase of nonradiative lifetime in thin shell CQDs may be due to the larger lattice mismatch between CdSe and ZnS (12%) [27]. This lattice mismatch creates additional defects in core-shell interface, providing poor confinement to excitons in thinner shells [45]. The decrease of nonradiative lifetime of core-shell CQDs with increase of shell thickness may be due to the thicker shells giving superior confinement to excitons [45]. For core-only CQDs, according to the data showing in Table 3, fluorescence lifetime, radiative lifetime and nonradiative lifetime increased with the increase of CQD size. This may be due to the lowering of band gap energy with the increase of CQD size, which facilitates the excitation of more excitons to higher excitation states, hence an increase of fluorescence life time and radiative lifetime. Further, this may also be due to the less e^-/h^+ overlap with the increase of CQD size resulting less surface interactions. The increase of nonradiative lifetimes of core-only materials may be due to increase interactions with surface capping ligand which can make dangling bonds between surface Se atoms and facilitate nonradiative emissions. This suggests that shell thickness has great influence on photophysical dynamics of core-shell CQDs.

Table 4
Calculated radiative and nonradiative rate constants for CQD samples.

Sample	k_r / s^{-1}	k_{nr} / s^{-1}
CSE500	7.90×10^8	9.43×10^8
CSE540	3.06×10^8	3.19×10^8
CSE580	3.57×10^7	7.06×10^7
CSE600	2.30×10^7	4.84×10^7
CSE620	3.90×10^7	5.90×10^7
CSE640	9.36×10^6	1.45×10^7
CZ500	5.70×10^7	3.73×10^7
CZ540	3.62×10^7	2.03×10^7
CZ580	1.22×10^7	1.20×10^7
CZ600	1.14×10^7	1.25×10^7
CZ620	1.00×10^7	1.65×10^7
CZ640	1.15×10^7	2.78×10^7

For better interpretation of our findings, the radiative rate constants (k_r) and nonradiative rate constants (k_{nr}) were calculated using lifetime data showing in Table 3. These calculated rate constants are provided in the Table 4.

According to Table 4, the nonradiative rate constants for core-only materials are larger compared to core-shell materials and it is clear that the shell helps to diminish the nonradiative pathways, making more photo stable cores. However, after certain shell thickness, the nonradiative decay constants increased gradually. As we discussed before, that may be due to the large lattice mismatch of CdSe/ZnS core-shell CQD, there may be a non-uniformity on shells with defects on shell surfaces [38,44]. We believe thicker shells cause to enhance trap emissions, distorting CdSe spherical core symmetry [24] which implies the increase of radiative lifetimes. Non-uniformity of shells can make dangling bonds with surface ligands and elongating bonds, which all facilitate the decrease of PL quantum yields by creating more defects, vacancies on the CQD surfaces. Furthermore, elongation of bonds may be caused to non-radiative vibrational energy transfer processes to the surface ligand which shows by slightly enhancing the nonradiative rate constants in Table 4. However, with the increase of nonradiative rate constant, the PL quantum yield is supposed to decrease but for our studies, according to the data shown in Table 4, radiative rate constants also increase simultaneously with the increase of nonradiative rate constants. Hence we are not observing a considerable change of PL quantum yields with increase of nonradiative rate constants.

The TCSPC data shows longer fluorescence lifetime for core-shell materials with compared to core-only materials. This is true because shells can passivate non-radiative trap sites and defects on the core and also promote radiative processes which we discussed before.

In comparison to the CdSe CQD samples, we observed that CdSe/ZnS core-shell materials showed a longer rise times. This is mainly due to the surface passivation of non-radiative emitting sites, avoiding oxidation of surface Se atoms and also enhancing the exciton generation on nano crystal surfaces by ZnS shell. According to the graphs on Fig. 3,

Table 5
Calculated rise time of CdSe (CSE) and CdSe/ZnS (CZ).

Sample	Rise time / ps	Sample	Rise time / ps
CSE500	0.57	**CZ500**	0.58
CSE540	0.52	**CZ540**	1.62
CSE580	0.58	**CZ580**	0.99
CSE600	0.81	**CZ600**	1.45
CSE620	0.49	**CZ620**	1.02
CSE640	0.76	**CZ640**	1.02

CdSe CQDs excite at 400 nm (3.102 eV) and show short rise times averaging of 0.62 ps. However, CdSe/ZnS CQDs show longer rise times with an average of 1.11 ps due to the shell hindering the fast decay components in the core. This make stable surfaces towards photo-oxidation, avoiding defects emissions and nonradiative e^-/h^+ recombination on the core surface. The calculated rise times for CdSe and CdSe/ZnS CQD samples are listed in the Table 5.

Although we are not observing a good correlation between the rise times and the size distribution of CQDs mentioned in Table 4, we can see in core-shell materials, a saturation of excitons after a certain shell thickness. As shown in Table 5, CZ620 and CZ640 show approximately the same rise times. This suggests that after a certain shell thickness, excitons cannot excite to a higher excitation state. Thicker shells may hinder further excitations to higher energy states.

5. Conclusion

In conclusion, we have successfully studied and, for the first time, reported the data on ODA capped CdSe and CdSe/ZnS CQDs. The studies show that, I) the higher excitation, photoinduced dynamics vary in core-only and core-shell materials, II) the effect of the size of CQDs on the higher excitation fluorescence decay dynamics, and III) the influence of the shell thickness on the fluorescence decay dynamics in CdSe/ZnS core-shell CQDs utilizing femtosecond, time-resolved fluorescence upconversion spectroscopy. The CdSe CQDs with the ZnS shell show good photostability and a large rising time due to passivation of the core by the ZnS shell, which creates stable surfaces for photo–oxidation and diminishing of nonradiative emissions on the core surface. In this study, we are able to show the way shell thickness affects photostability and photophysical dynamics of these core-shell CQD materials by enhancing radiative lifetimes and diminishing nonradiative lifetimes due to the passivation of non-radiative trap sites on CdSe cores using fluorescence decay studies. Further, we are able to show the shell thickness dependence photophysical dynamics of these CQDs probing the fluorescence decay dynamics. According to the best of our knowledge, this is the first time reporting the effects of shell thickness on core-shell CQDs using a systematic comparative study of fluorescence decay dynamics of core and core-shell CQDs.

In the literature, it has been shown that different dimensions of core-shell CQD change their photoinduced dynamics with the shell thickness [46]. We are continuing our investigations to understand the effect of different geometries of core-shell materials on the photoinduced dynamics of CQDs.

Acknowledgments

The MIR wishes to thank NSF for funding support through NM-EPSCOR solar energy nexus (#IIA-1301346). NMT start up grant also contributed to establishing the “ultrafast laser spectroscopy facility”. We also wish to thank Professor Michael D. Heagy of NMT for his support.

References

[1] A.M. Smith, S. Nie, Semiconductor nanocrystals: structure, properties, and band gap engineering, Acc. Chem. Res. 43 (2010) 190–200.
[2] B.O. Dabbousi, J. Rodriguez-Viejo, F.V. Mikulec, J.R. Heine, H. Mattoussi, R. Ober, K.F. Jensen, M.G. Bawendi, (CdSe)ZnS core-shell quantum dots: synthesis and characterization of a size series of highly luminescent nanocrystallites, J. Phys. Chem. B 101 (1997) 9463–9475.
[3] D. Vasudevan, R.R. Gaddam, A. Trinchi, I. Cole, Core–shell quantum dots: properties and applications, J. Alloy. Compd. 636 (2015) 395–404.
[4] G.H. Carey, A.L. Abdelhady, Z. Ning, S.M. Thon, O.M. Bakr, E.H. Sargent, Colloidal quantum dot solar cells, Chem. Rev. 115 (2015) 12732–12763.
[5] M. Kouhnavard, S. Ikeda, N.A. Ludin, N.B. Ahmad Khairudin, B.V. Ghaffari, M.A. Mat-Teridi, M.A. Ibrahim, S. Sepeai, K. Sopian, A review of semiconductor materials as sensitizers for quantum dot-sensitized solar cells, Renew. Sustain. Energy Rev. 37 (2014) 397–407.
[6] H.K. Jun, M.A. Careem, A.K. Arof, Quantum dot-sensitized solar cells—perspective and recent developments: a review of Cd chalcogenide quantum dots as sensitizers, Renew. Sustain. Energy Rev. 22 (2013) 148–167.
[7] P.V. Kamat, Quantum dot solar cells. Semiconductor nanocrystals as light harvesters, J. Phys. Chem. C 112 (2008) 18737–18753.
[8] D.F. Underwood, T. Kippeny, S.J. Rosenthal, Charge carrier dynamics in CdSe nanocrystals: implications for the use of quantum dots in novel photovoltaics, Eur. Phys. J. D - At., Mol., Opt. Plasma Phys. 16 (2001) 241–244.
[9] J.B. Sambur, T. Novet, B.A. Parkinson, Multiple exciton collection in a sensitized photovoltaic system, Science 330 (2010) 63–66.
[10] M.J. Bowers, Ii, J.R. McBride, M.D. Garrett, J.A. Sammons, A.D. Dukes Iii, M.A. Schreuder, T.L. Watt, A.R. Lupini, S.J. Pennycook, S.J. Rosenthal, Structure and ultrafast dynamics of white-light-emitting cdse nanocrystals, J. Am. Chem. Soc. 131 (2009) 5730–5731.
[11] M.J. Bowers, J.R. McBride, S.J. Rosenthal, White-light emission from magic-sized cadmium selenide nanocrystals, J. Am. Chem. Soc. 127 (2005) 15378–15379.
[12] W.K. Bae, S. Brovelli, V.I. Klimov, Spectroscopic insights into the performance of quantum dot light-emitting diodes, MRS Bull. 38 (2013) 721–730.
[13] S. Brovelli, W.K. Bae, C. Galland, U. Giovanella, F. Meinardi, V.I. Klimov, Dual-color electroluminescence from dot-in-bulk nanocrystals, Nano Lett. 14 (2014) 486–494.
[14] B.A. Kairdolf, A.M. Smith, T.H. Stokes, M.D. Wang, A.N. Young, S. Nie, Semiconductor quantum dots for bioimaging and biodiagnostic applications, Annu. Rev. Anal. Chem. (Palo Alto, Calif.) 6 (2013) 143–162.
[15] M. Bruchez, M. Moronne, P. Gin, S. Weiss, A.P. Alivisatos, Semiconductor nanocrystals as fluorescent biological labels, Science 281 (1998) 2013–2016.
[16] S.J. Rosenthal, I. Tomlinson, E.M. Adkins, S. Schroeter, S. Adams, L. Swafford, J. McBride, Y. Wang, L.J. DeFelice, R.D. Blakely, Targeting cell surface receptors with ligand-conjugated nanocrystals, J. Am. Chem. Soc. 124 (2002) 4586–4594.
[17] C. Burda, T.C. Green, S. Link, M.A. El-Sayed, Electron Shuttling Across the Interface of CdSe Nanoparticles Monitored by Femtosecond Laser Spectroscopy, J. Phys. Chem. B 103 (1999) 1783–1788.
[18] M. Jones, S.S. Lo, G.D. Scholes, Quantitative modeling of the role of surface traps in CdSe/CdS/ZnS nanocrystal photoluminescence decay dynamics, Proc. Natl. Acad. Sci. 106 (2009) 3011–3016.
[19] M. Jones, S.S. Lo, G.D. Scholes, Signatures of exciton dynamics and carrier trapping in the time-resolved photoluminescence of colloidal CdSe nanocrystals, J. Phys. Chem. C 113 (2009) 18632–18642.
[20] S. Jeong, M. Achermann, J. Nanda, S. Ivanov, V.I. Klimov, J.A. Hollingsworth, Effect of the Thiol − Thiolate equilibrium on the photophysical properties of aqueous CdSe/ZnS nanocrystal quantum dots, J. Am. Chem. Soc. 127 (2005) 10126–10127.
[21] V.I. Klimov, A.A. Mikhailovsky, D.W. McBranch, C.A. Leatherdale, M.G. Bawendi, Quantization of multiparticle auger rates in semiconductor quantum dots, Science 287 (2000) 1011–1013.
[22] M.A. Hines, P. Guyot-Sionnest, Synthesis and characterization of strongly luminescing ZnS-capped cdse nanocrystals, J. Phys. Chem. 100 (1996) 468–471.
[23] N. Lenngren, M.A. Abdellah, K. Zheng, M.J. Al-Marri, D. Zigmantas, K. Zidek, T. Pullerits, Hot electron and hole dynamics in thiol-capped CdSe quantum dots revealed by 2D electronic spectroscopy, Phys. Chem. Chem. Phys. 18 (2016) 26199–26204.
[24] S. Mathew, B.S. Bhardwaj, A.D. Saran, P. Radhakrishnan, V.P.N. Nampoori, C.P.G. Vallabhan, J.R. Bellare, Effect of ZnS shell on optical properties of CdSe–ZnS core–shell quantum dots, Opt. Mater. 39 (2015) 46–51.
[25] Z. Yu, L. Guo, H. Du, T. Krauss, J. Silcox, Shell distribution on colloidal CdSe/ZnS quantum dots, Nano Lett. 5 (2005) 565–570.
[26] H. Zhu, N. Song, T. Lian, Controlling charge separation and recombination rates in CdSe/ZnS Type I core − shell quantum dots by shell thicknesses, J. Am. Chem. Soc. 132 (2010) 15038–15045.
[27] T.C. Kippeny, M.J. Bowers, A.D. Dukes, J.R. McBride, R.L. Orndorff, M.D. Garrett, S.J. Rosenthal, Effects of surface passivation on the exciton dynamics of CdSe nanocrystals as observed by ultrafast fluorescence upconversion spectroscopy, J. Chem. Phys. 128 (2008) 084713.
[28] D.F. Underwood, T. Kippeny, S.J. Rosenthal, Ultrafast carrier dynamics in cdse nanocrystals determined by femtosecond fluorescence upconversion spectroscopy, J. Phys. Chem. B 105 (2001) 436–443.
[29] A. Makhal, H. Yan, P. Lemmens, S.K. Pal, Light harvesting semiconductor core − - shell nanocrystals: ultrafast charge transport dynamics of CdSe-ZnS quantum dots, J. Phys. Chem. C 114 (2010) 627–632.
[30] M.A. Kahlow, Wo Jarzęba, T.P. DuBruil, P.F. Barbara, Ultrafast emission spectroscopy in the ultraviolet by time-gated upconversion, Rev. Sci. Instrum. 59 (1988) 1098–1109.
[31] M.D. Garrett, M.J. Bowers, J.R. McBride, R.L. Orndorff, S.J. Pennycook, S.J. Rosenthal, Band edge dynamics in CdSe nanocrystals observed by ultrafast

fluorescence upconversion, J. Phys. Chem. C 112 (2008) 436–442.
[32] A. Piryatinski, S.A. Ivanov, S. Tretiak, V.I. Klimov, Effect of quantum and dielectric confinement on the exciton-exciton interaction energy in type II core/shell semiconductor nanocrystals, Nano Lett. 7 (2007) 108–115.
[33] J.T. Stewart, L.A. Padilha, W.K. Bae, W.-K. Koh, J.M. Pietryga, V.I. Klimov, Multiplication in quantum dots within the framework of two competing energy relaxation mechanisms, J. Phys. Chem. Lett. 4 (2013) 2061–2068.
[34] L.A. Padilha, J.T. Stewart, R.L. Sandberg, W.K. Bae, W.-K. Koh, J.M. Pietryga, V.I. Klimov, Carrier multiplication in semiconductor nanocrystals: influence of size, shape, and composition, Acc. Chem. Res. 46 (2013) 1261–1269.
[35] J. Lim, B.G. Jeong, M. Park, J.K. Kim, J.M. Pietryga, Y.-S. Park, V.I. Klimov, C. Lee, D.C. Lee, W.K. Bae, Influence of shell thickness on the performance of light-emitting devices based on CdSe/Zn1-XCdXS Core/Shell heterostructured quantum dots, Adv. Mater. 26 (2014) 8034–8040.
[36] C.M. Cirloganu, L.A. Padilha, Q. Lin, N.S. Makarov, K.A. Velizhanin, H. Luo, I. Robel, J.M. Pietryga, V.I. Klimov, Enhanced carrier multiplication in engineered quasi-type-II quantum dots, Nat. Commun. 5 (2014) 4148.
[37] C. Burda, X. Chen, R. Narayanan, M.A. El-Sayed, Chemistry and properties of nanocrystals of different shapes, Chem. Rev. 105 (2005) 1025–1102.
[38] X. Chen, Y. Lou, A.C. Samia, C. Burda, Coherency strain effects on the optical response of core/shell heteronanostructures, Nano Lett. 3 (2003) 799–803.
[39] Y. Kobayashi, C.-H. Chuang, C. Burda, G.D. Scholes, Exploring ultrafast electronic processes of quasi-type II nanocrystals by two-dimensional electronic spectroscopy, J. Phys. Chem. C 118 (2014) 16255–16263.
[40] D.M. Mittleman, R.W. Schoenlein, J.J. Shiang, V.L. Colvin, A.P. Alivisatos, C.V. Shank, Quantum size dependence of femtosecond electronic dephasing and vibrational dynamics in CdSe nanocrystals, Phys. Rev. B 49 (1994) 14435–14447.
[41] J.B. Sambur, B.A. Parkinson, CdSe/ZnS core/shell quantum dot sensitization of low index TiO2 single crystal surfaces, J. Am. Chem. Soc. 132 (2010) 2130–2131.
[42] M. Grabolle, J. Ziegler, A. Merkulov, T. Nann, U. Resch-Genger, Stability and fluorescence quantum yield of CdSe–ZnS quantum dots—influence of the thickness of the ZnS shell, Ann. New Y. Acad. Sci. 1130 (2008) 235–241.
[43] D.-S. Liang, L. Shen, Z.-B. Wang, Y.-P. Cui, J.-Y. Zhang, Y.-H. Ye, Evolution of luminescence with shell's thickness in colloidal CdSe/CdS, Chin. Phys. Lett. 25 (2008) 4431.
[44] B. Omogo, F. Gao, P. Bajwa, M. Kaneko, C.D. Heyes, Reducing blinking in small core–multishell quantum dots by carefully balancing confinement potential and induced lattice strain: the “Goldilocks” effect, ACS Nano 10 (2016) 4072–4082.
[45] J. Bleuse, S. Carayon, P. Reiss, Optical properties of core/multishell CdSe/Zn(S,Se) nanocrystals, Phys. E: Low.-Dimens. Syst. Nanostruct. 21 (2004) 331–335.
[46] A. Kar, Q. Li, P.C. Upadhya, M. Ah Seo, J. Wright, T.S. Luk, G.T. Wang, R.P. Prasankumar, The influence of radial heterostructuring on carrier dynamics in gallium nitride nanowires, Appl. Phys. Lett. 101 (2012) 143104.